Chapter 5

a-Si:H p-i-n Photodiode as a Biosensor

Vera Gradišnik and Darko Gumbarević

Additional information is available at the end of the chapter

http://dx.doi.org/10.5772/intechopen.80503

Abstract

The p-i-n a-Si:H photodiode is a promising device as a transducer in biosensors. The native and light-induced localized state density and energy distribution in the energy gap of a-Si:H have a large effect on the photoconductivity of thin-film photodiodes. Depending on their nature, they play a crucial role in trapping and recombination processes and consequently influence the photodiode capacitance. The optical bias dependence of modulated photocurrent, OBMPC, method using the blue LED light is applied to clarify the nature and energy distribution of the energy gap density of states and their influence on the photodiode capacitance, from photodiodes transient response. It is observed that the deep defect states of the i-layer contribute to the capacitance at various bias voltages. Also, the capacitance achieves the upper limit around the built-in potential. Based on this method and obtained results, the a-Si:H p-i-n photodiode is used as a biosensor transducer in the detection of mammalian cell chemiluminescence.

Keywords: a-Si:H p-i-n photodiode, biosensor, blue light, capacitance, defects, density of states, LED, transient response

1. Introduction

The recent advances, miniaturization and integration, in nanotechnology and CMOS technology afforded by photolithographic patterning, have had a transformative impact on the field of single-cell biology and diseases that depend on small collections of cells in their initial stages such as cancer. The microfluidic Lab-on-a-chip technology, still under development, meets point-of-care (POC) requirements for biomolecular analyses. The biosensors consisting of amorphous silicon (a-Si:H) p-i-n photodiode as integrated luminescence sensor in lab-on-a-chip devices, coupled with a microLED, have progressed rapidly over the last two decades and are still under development [1, 2]. The a-Si:H p-i-n photodiode is widely used as a transducer

in biosensors for biochemical analysis, where are applied pico- to nano-liters (microliters) of volumes of fluids in channels of tens to hundreds of micrometers. The photodiode array must have very high detection precision and allow conducting parallel experiments for the detection of biomolecules. Biosensor response must satisfy the main performance criteria: selectivity, sensitivity, linearity, and response time. At the same time, the photonic method for measuring the oxygen consumption rate (OCR) of a single cell must be developed.

The sensitivity of thin-film a-Si:H p-i-n photodiodes, integrated with microfluidics, allows low-level luminescence signal detection from the volume of a microfluidic channel. The thin-film hydrogenated amorphous silicon (a-Si:H) technology [3] allows the custom fit of amorphous silicon photodiode arrays to the geometry of the flow microfluidic channel. The low-temperature (below 200°C) technology plasma-enhanced chemical-vapor deposition (PECVD) [2] or hot wire chemical-vapor deposition (HWCVD) [4] allows deposition of amorphous layers on the glass and polymer substrates, respectively, and on top of crystalline silicon integrated circuits without any damage to the circuits below [5]. At appropriate RF power, gas flows, chamber pressure, and substrate temperature in PECVD, hydrogen atoms are introduced into the thin film to passivate the silicon dangling bonds (DBs) and remove a part of (metastable) defect states from the forbidden band gap. In pure amorphous silicon, unsaturated dangling bonds (DBs) give rise to electronic states inside the band gap. The hydrogen atoms restore the energy gap and semiconductor properties. Due to the disordered structure alloying virtually all optical transitions, the absorption coefficient of a-Si:H is higher than that of c-Si (500–650 nm) [6]. Besides, a much lower dark current of a-Si:H than c-Si at room temperature enables its use as a photodiode material for low-noise detection. The photodiodes, as part of active area in active pixel sensors (APSs) [7–10] and other devices based on amorphous silicon, recently entered the field of microelectronics. The main part of applications was directed toward steady-state illumination of slowly varying light signals. The transient photocurrent was used for the material properties characterization and color detection [11–13].

The amorphous silicon photodiode can operate in integrated and in a reverse-biased photodiode mode. In the latter, they have a high response speed and the photocurrent is only controlled by the light intensity. In amorphous silicon, the transport of free carriers involves trapping, detrapping through a large density of midgap states (DOS), and motion through transport in the extended states—localized band tail state [14]. These native and light-induced densities of state and their energy distribution in the energy gap of a-Si:H have a large effect on the photoconductivity of thin-film photodiodes. Depending on their nature, they play a crucial role in trapping and recombination processes and consequently influence the photodiode capacitance and relaxation time. Furthermore, they lead to a high RC constant of a thin-film a-Si:H photodiode.

The disordered structure of hydrogenated amorphous silicon (a-Si:H) leads to localized states as band tails that extend inside the energy gap. The coordination defects associated with dangling bonds are sources of defect states located around the midgap. The tail states are shallow states, and the dangling bonds, the deep states. Both of them influence the recombination processes, capture and reemission of carriers in semiconductor. The emission of free charge carriers from deep states at the p-i and i-n interfaces influences the dark current, space

charge inside i-layer, and capacitance. The concentration of midgap states and their spatial distribution in the i-layer and at p^+-i and n^+-i interfaces can be extracted from transient dark current and steady-state thermal generation current, as described by Murthy and Dutta, and by Mahmood and Kabir [15, 16]. Models of transport and recombination through localized states have also been well described by Fuhs [14] and Dhariwal et al. [17–19]. Several techniques based on steady-state and transient photocurrent techniques have been developed to determine the nature and role of gap density of states (DOS) in the trapping-detrapping, recombination processes of mobile carriers and gap-state parameters [20]. To estimate the DOS in the lower part of band gap between the Fermi level and valence band edge, methods such as constant photocurrent method (CPM) [21], Fourier transform photocurrent spectroscopy (FTPS) [22, 23], and dual beam photoconductivity (DBP) [24] were used in the past. On the other hand, the multiexponential trapping rate and modulated photocurrent (MPC) technique [25–27] allow determining parameters of localized states throughout the entire energy gap by employing frequency and temperature scans.

The aim of our research is the mammalian cells chemiluminescence detection, which is based on the phenomenon that under illumination of two-beam, low intensity probe beam and simultaneously a higher intensity bias beam, reverse-biased a-Si:H p-i-n photodiode photocurrent exceed expected primary photocurrent [26].

The transient response of a-Si:H p-i-n photodiode to blue LED light pulse superimposed to the blue LED light optical bias (optical bias dependence of modulated photocurrent method—OBMPC [11, 27]) at various reverse bias voltages and one frequency is applied to clarify the nature and energy distribution of energy gap density of state and their influence on the photodiode capacitance [28]. It is observed that the deep defect states of the i-layer contribute to the capacitance at various bias voltages. Also, the capacitance achieves the upper limit around the built-in potential.

Based on this method and obtained results, we describe our experiment, where the a-Si:H p-i-n photodiode is used as a biosensor transducer in the detection of mammalian cell's chemiluminescence.

2. a-Si:H p-i-n photodiode

2.1. Device structure and characterization

The fundamental structure of a photodiode in amorphous silicon is p-i-n or n-i-p. The a-Si:H p-i-n structure (**Figure 1**) investigated in this work (Sunčane ćelije d.o.o. Split, Croatia) was deposited on a transparent conductive oxide (TCO)-coated glass from undiluted SiH_4 by plasma-enhanced CVD at 13.56 MHz. The different layers of the p-i-n structure have the parameters of standard solar cell production. The thicknesses of the n-type, i-type, and p-type layers were 5, 300, and 5 nm, from top to the bottom, respectively. The n-type layer was made by adding phosphine PH_3 and the p-type by adding diborane B_2H_6 into the silane SiH_4 source gas during growth. The back contact was aluminum deposited by evaporation.

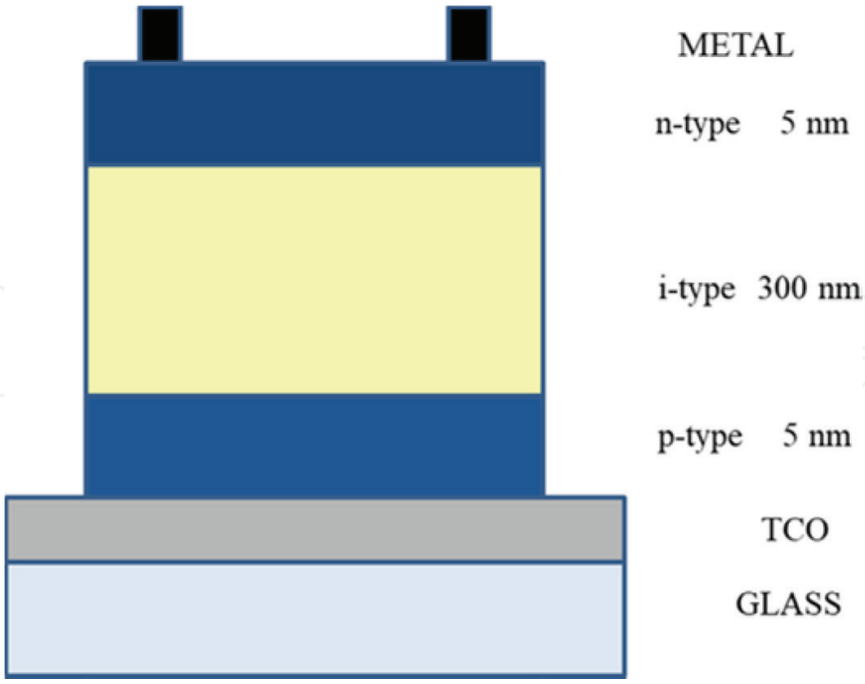

Figure 1. The a-Si:H p-i-n photodiode structure.

The active area of the pixel was 0.81 cm^2. The basic device characterization and experimental system are described in more detail in [12, 13]. Photoillumination was obtained through the bottom p-type layer.

The doped layers in a-Si:H are nearly transparent to visible light and should be as thin as possible to minimize parasitic absorption. The minority carriers have small diffusion lengths; therefore, n-type and p-type a-Si:H are not photoactive layers. The i-layer is a region with high electric field. The light is mostly absorbed in the intrinsic i-layer, where the photo-generation occurs. The photocarriers at reverse bias voltages are swept away by the electric field in the i-layer, electrons to the n-type and holes to the p-type, and contribute mainly to drift photocurrent. Dark current increases with bias voltage as shown in **Figure 2**. It is very small in a-Si:H devices at low bias voltages and is given by thermal carrier emission from the bulk. With increased bias voltage, the injection from the doped layer increases too [15]. The signal current should be much higher than the leakage (dark) current at applied reverse bias voltage at which the electric filed, necessary to achieve full depletion inside the i-layer, collects all the photo-generated e-h pairs. At the same time, the absorbed light creates additional defects.

Defects in amorphous silicon lead to a low mobility of the charge carriers. The recombination losses of free carriers, trapping-detrapping in midgap states, and band tail states lead to photo-generated space charge in the i-layer. The space charge distribution at the p-i edge and at the n-i edge influences the internal field and screens the applied field. It is associated with the electrons and holes' capacitance in the series. In amorphous silicon, the localized states arise from their disordered nature, bond lengths, and angles between the silicon atoms. The broken or dangling bonds (DBs) arise from not-satisfied Si-Si bonds. To passivate those DBs in material is introduced the hydrogen to form the chemical bonds with the defects.

http://dx.doi.org/10.5772/intechopen.80503

The H content in the material influences the band gap values which are typically around 1.7–1.8 eV. These metastable localized states act as defect (D) states at discrete energies and as recombination centers. Dangling bonds are the main defect in a-Si:H and have defect pool model distribution and Gaussian distribution (**Figure 3**) [27]. They can be in neutral $D^0(E)$, positive $D^+(E)$, and negative $D^-(E)$ charge states and their distributions depend on light intensity and temperature. The transition $D^{+/0}$ follows acceptor statistics and $D^{0/-}$ donor statistics.

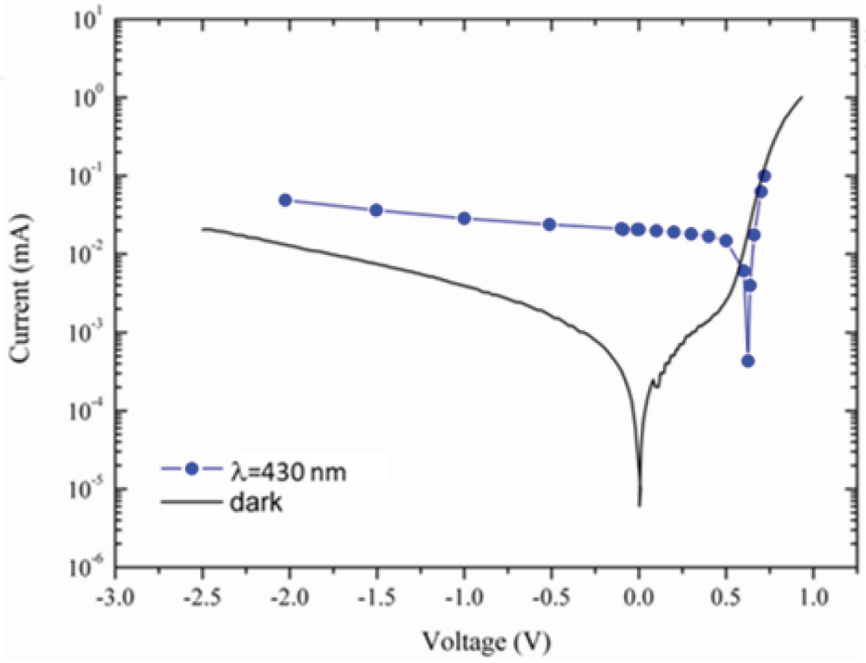

Figure 2. The p-i-n a-Si:H PD current-voltage, I-V, characteristics measured under the dark and blue LED light illumination, λ = 430 nm.

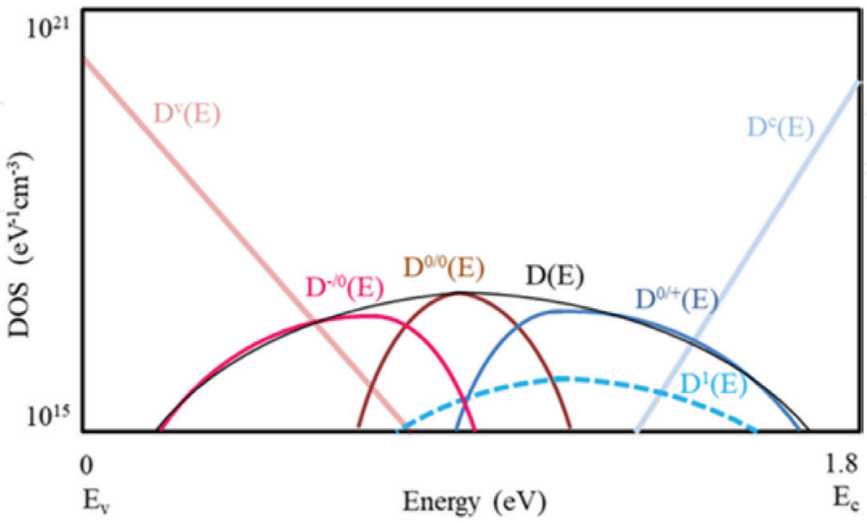

Figure 3. Scheme of band tail distribution (Dv, Dc), DOS equilibrium distribution according to defect pool model, and $D^1(E)$ acceptor-like Gaussian distribution after [27].

In a-Si:H, electrons occupying the localized states are trapped or immobile, and electrons occupying extended states are assumed to be mobile and are characterized by a "band mobility" ($\mu_n \simeq 10\,\mathrm{cm^2\,s^{-1}}$). The localized band tail states are divided from extended electron states by E_C conduction mobility edge. There are the valence mobility-edge E_V separating delocalized transport states (below E_V), where the free holes are characterized by a "band mobility" ($\mu_p \simeq 1\ \mathrm{cm^2\,s^{-1}}$), and localized traps (above E_V). The band tail states have an exponential distribution ("Urbach" tail). The conduction band tail (acceptor type) width is assumed to be $\Delta E_C = 25\,\mathrm{eV}$ and the valence band tail (donor type) width $\Delta E_V = 45 - 50\ \mathrm{meV}$, respectively. Hence, in a-Si:H, the mobility gap denotes the switch from small to larger mobility.

The localized state density (DOS) is so large that an electron can move from one localized site to another by hopping and the transport via these gap states is possible, but usually in numerical analysis it is neglected. The DBs act as main recombination centers. The empty gap states (trap) which interact with majority carriers via trapping-detrapping processes can be probed under sufficiently weak bias illumination level and high modulation frequency MPC method [27]. At low frequency regime, the recombination of free electrons through the recombination centers in gap distributions D(E) occupied by holes between the trap quasi-Fermi levels of electrons and holes can be probed depending on the magnitude of the capture coefficients of the recombination centers. The scheme of the DOS distribution in undoped a-Si:H, according to the defect pool model and Gaussian distribution, is shown in **Figure 3**.

Han et al. [29] have reported the most interesting feature of optical bias. Optical bias impedes deep trapping, thus enhancing electron drift. Their photocapacitance and capacitance transient measurement result indicates the band tail transport occurs in time shorter than 10 μs which is not affected by optical bias, electron trapping, and further drift following reemission from the deep trap in time longer than 1 ms.

To use the a-Si:H p-i-n photodiode as a biosensor transducer in detection of mammalian HeLa cells' chemiluminescence in our main experiment, the photodiode characterization is first done. All measurements were performed at the room temperature. LEDs (Kingbright) emitting at 430 nm for blue (B) were used in the experiment and the dc forward current through the LED was I_F = 20 mA. The energy of monochromatic LED light is higher than the band gap energy.

The photodiode current-voltage (I-V) characteristics measured under the dark and blue LED light illumination at λ = 430 nm are shown in **Figure 2**. Under low forward voltages, the dark current is dominated by Shockley-Read-Hall (SRH) recombination [30].

In order to obtain the information on the recombination rate in dark, the ideality factor is studied. It is well known that in a-Si:H, the ideality factor is a non-integer and decreases with temperature [30].

The recombination rate depends on the concentration of active recombination centers which include all traps between the quasi-Fermi levels for trapped charges. Second, it depends on the recombination efficacy of each of these recombination centers. These two factors are voltage dependent due to the continuous density of states in the band gap. The dark current has an exponential term and the integration term. The exponential term with ideality factor n = 2

is due to the injection of free carriers, electrons and holes, from the n and p contacts, and their recombination through a single defect level. The integration term is due to the number of defect states which act as recombination centers and are located between the quasi-Fermi levels for trapped holes, E_{fp_t}, and trapped electrons, E_{fn_t}. Their concentrations increase with increased applied voltage, as the separation of quasi-Fermi levels increases.

From dark current-voltage characteristics

$$I(V) = \mathrm{I}_0 \exp\left(\frac{\mathrm{qV}}{\mathrm{nkT}}\right) \tag{1}$$

and the ideality factor defined by Deng and Wronski [31] is

$$n(V) = \left[\frac{\mathrm{kT}}{q}\frac{\mathrm{dln}(I_D)}{\mathrm{dV}}\right]^{-1}. \tag{2}$$

The shape of the $n(V)$ curve, shown in **Figure 4**, reflects the energy distribution, as a Gaussian one, of the defect states in the *i*-layer.

The total recombination current density conducted through the device expressed by its activation energy of SRH recombination [30] shown in **Figure 5** is calculated by the expression:

$$E_a^R(V) = \frac{E_\mu - V}{2} + 3kT \tag{3}$$

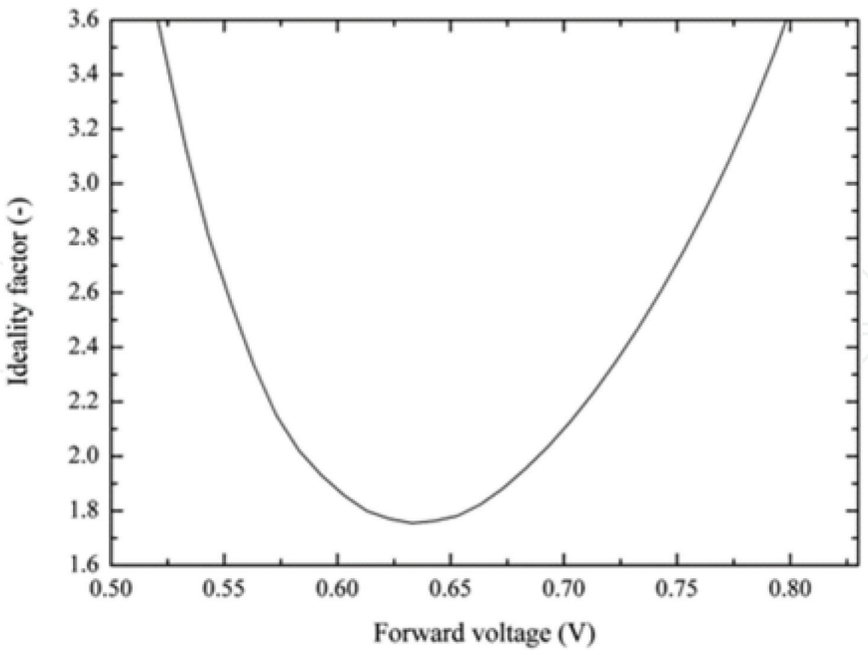

Figure 4. The voltage-dependent ideality factor, $n(V)$, as a function of voltage at room temperature for a p-i-n photodiode with an i-layer thickness of 300 nm. Calculation is done using the Deng and Wronski definition of voltage-dependent ideality factor.

where E_μ is mobility gap and V the applied voltage. Calculation is done following the Kind et al. expression for the voltage-dependent activation energy of the total recombination at various mobility gap and voltage-dependent ideality factor values shown in **Figure 4**. For comparison is given the activation energy at constant ideality factor n = 2 (the thermal ideality factor defined by Pieters et al. and used in [30]).

2.2. Photodiode capacitance

The time domain technique at low frequency is used to measure the photodiode's capacitance [32]. The measurements have been carried out on a-Si:H p-i-n cells under forward and reverse bias voltages, in dark and upon blue LED illumination and voltage pulses at 333 Hz [33].

The total charge stored in photodiode capacitor depends on the photodiode voltage as described by

$$Q = \int_0^{V_{PD}} C_{PD}\, dV \tag{4}$$

where Q is the total charge stored, C_{PD} is the photodiode capacitance as a function of voltage, and V_{PD} is the voltage across the photodiode capacitance. The current due to stored charge is

$$i(t) = \frac{dQ}{dt}. \tag{5}$$

The charge equivalent linear capacitor C_q, which stores the same amount of charge as a photodiode capacitor at photodiode voltage $V_{PD,}$ is defined as

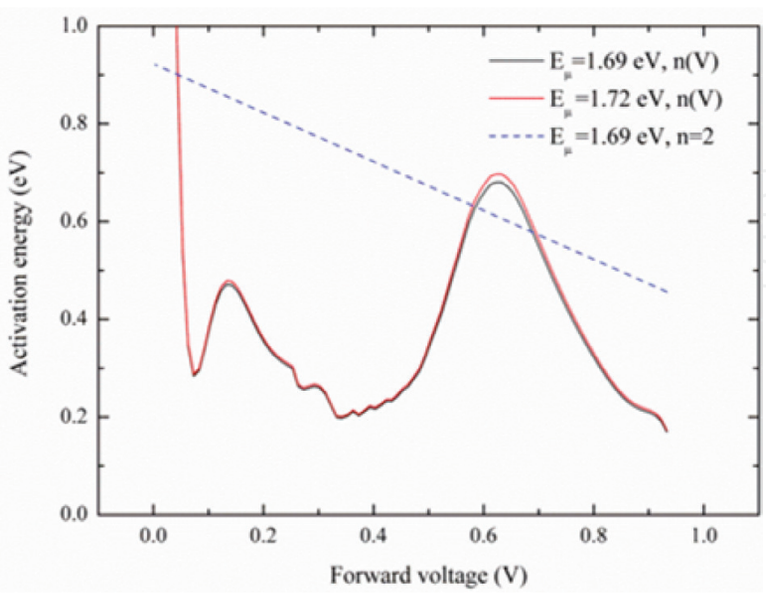

Figure 5. The activation energy as a function of voltage for an a-Si:H p-i-n photodiode with an i-layer thickness of 300 nm at room temperature.

http://dx.doi.org/10.5772/intechopen.80503

$$C_q = \frac{Q}{V_{PD}} = \frac{\int_0^{V_{PD}} idt}{V_{PD}} = \frac{\int_0^{V_{PD}} C_{PD}\, dv}{V_{PD}} \tag{6}$$

The photodiode current is measured with digital storage oscilloscope (Keysight InfiniiVision 2000 X-Series Oscilloscopes) by voltage drop across the resistor. The dc bias voltage (−2 to 0.7 V) is applied and measurements are carried out. The characteristic photodiode transient response on voltage pulse is shown in **Figure 6**. The cell capacitance is calculated from total charge obtained by integration of photodiode current transient response on voltage pulse Eq. (6) and divided with the corresponding photodiode bias voltage.

The dark capacitance's dependence on photodiode voltage and capacitance under illumination with blue light is shown in **Figure 7**. It shows a quasi-linear dependence of capacitance on the voltage under illumination.

It is observed that the deep defect states of the i-layer contribute to the capacitance at various bias voltages. It is evident that around the built-in voltage, the injected charge in the dark and photo-generated charge have the same value. At higher voltages prevails the injected charge in dark. Also, the capacitance achieves the upper limit around the built-in potential. The capacitance degradation effect happens at sufficiently high forward voltages around built-in voltage (V_{bi}), where the diode injection capacitance becomes more dominant and the device responds to the voltage as a resistor.

The area under the current response curve gives the total charge (**Figure 8**) accumulated in the photodiode. In dark, at reverse bias voltages higher than 0.5 V, the changes in space charge

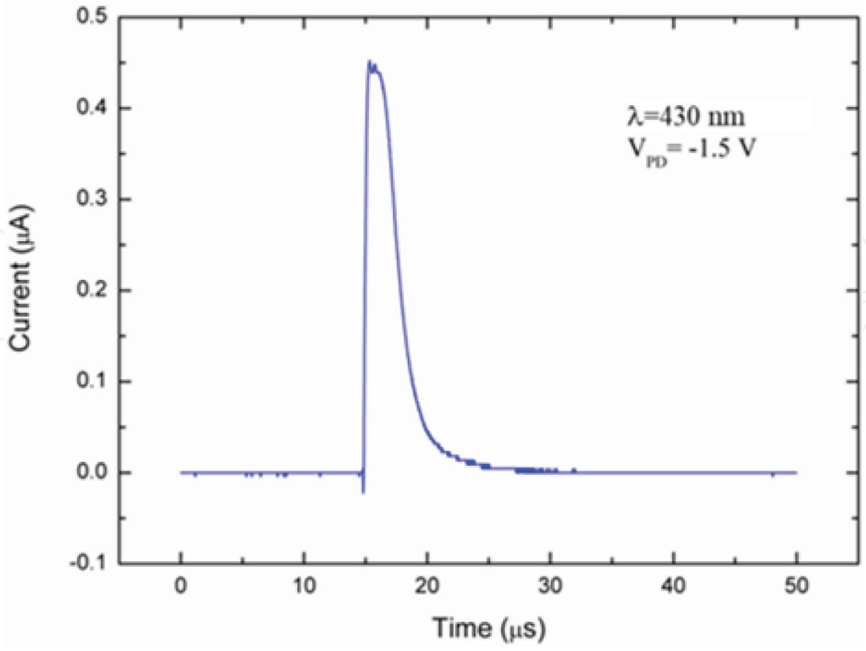

Figure 6. The transient response of a-Si:H photodiode to a square voltage pulse upon blue light illumination and reverse bias voltage V_{PD} = −1.5 V.

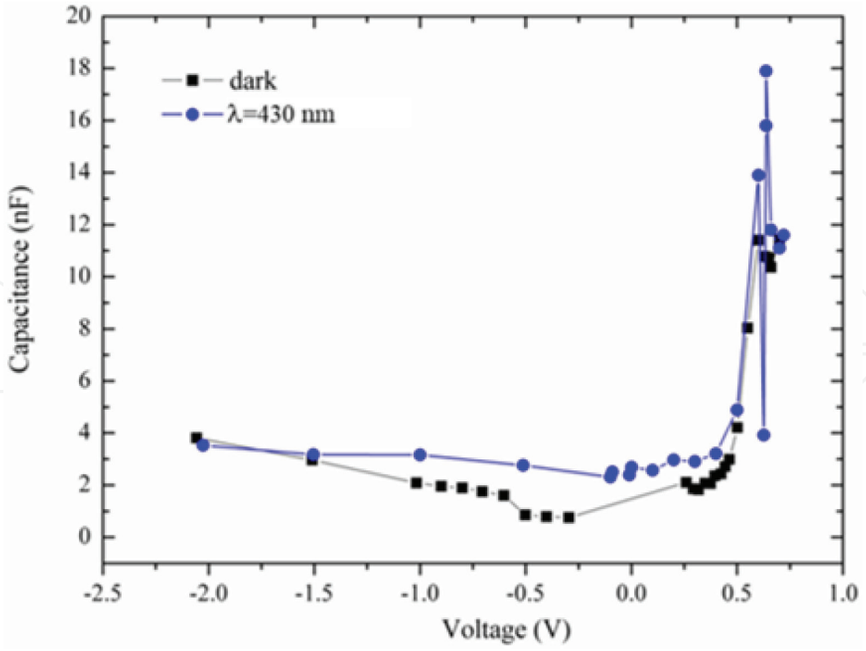

Figure 7. The a-Si:H photodiode capacitance versus bias photodiode voltages.

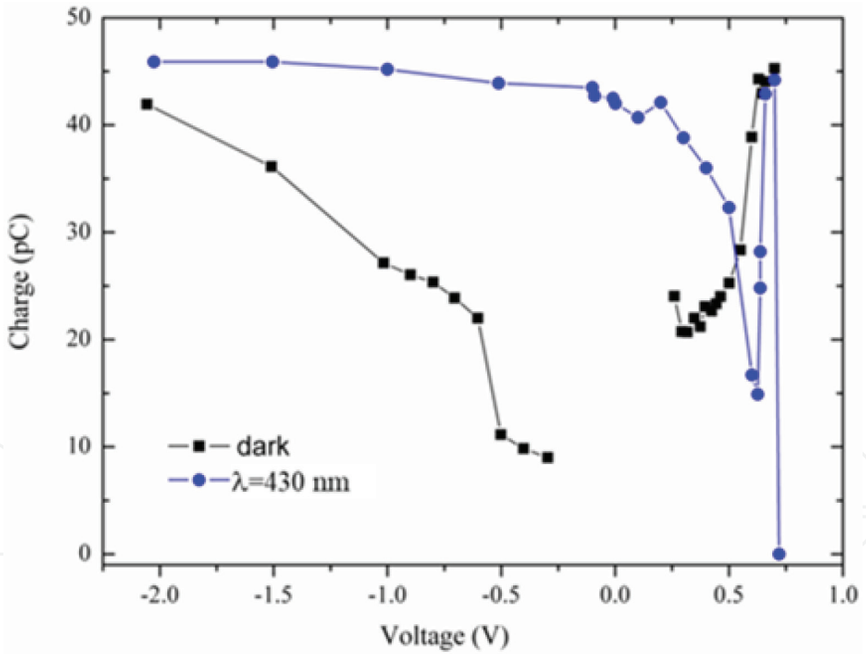

Figure 8. The a-Si:H photodiode total accumulated charge at different device voltages in dark and under blue LED light illumination (430 nm).

and local electric field in i-layer around p/i and n/i interfaces lead to the increase in total accumulated charge and consequently the capacitance increases. The increase in photo-generated charge with increased reverse bias voltage is smaller than dark charge. The proposed method can be used for further development of photodiode-integrated system and biosensors.

2.3. The blue light-induced defect creation examined with the OBMPC method

Using moderated OBMPC [11, 27, 36], we examine the light-induced defects kinetics and nature in the i-layer of a-Si:H p-i-n photodiode. Furthermore, we clarify their influence on photocurrent degradation and capacitance contribution.

The photodiode was illuminated with two blue LEDs (430 nm), a constant pump (optical bias) light and square pulse (probe) light at frequency of 333 Hz with 50% duty cycle. The intensity of the optical bias light and the pulsed probe beam was adjusted with 20-mA current through the LEDs. The illuminations were from the p-type layer side. The measurements were performed in the range from forward bias voltages of 0.7 V to reverse bias voltages of −2 V. From the measured switch-off transient response to a blue light pulse, we numerically analyze, by the generalized Foss method and general solution developed by Jeričević [33, 34], the trap and recombination localized states' energy distribution in the energy gap. The number of components, not known in advance, in multiexponential decay of measured switch-off transient response is determined by its best fit with numerically modeled transient response.

The photo-generated electron-hole pairs upon blue light illumination are nonuniformly generated near the front surface in the vicinity of the p^+/i interface. The photo-generated free carrier densities, electrons, and holes, have dc and time-dependent pulsed components.

The holes' contribution to the transient photocurrent is small, due to their trapping near the p^+/i interface where arises the space charge density or their movement into the front contact [11].

We observe a short time delay of transient photocurrent ascribed to trapping and release interaction of free carriers with shallow band gap localized states. The transient photocurrent decay in tail-like form, dependent on applied voltage, often happens due to deep trapping. It is dependent on the time that an electron spent in discrete localized states $N(E_i)$ at E_i energy levels (capture and release), as described in [11].

$$\tau = \nu_0^{-1} e^{(E_i/kT)}. \tag{7}$$

Based on the MPC theory described in [36], the band gap energy is divided into three energy ranges. The energies from which electrons (holes) can be trapped and released to the conduction (valence) band, E, are above, $E > E_{tn}$ (below, $E < E_{tp}$) quasi-Fermi level for trapped electrons, E_{tn} (trapped holes, E_{tp}), and recombination states between quasi-Fermi level for trapped electrons, E_{tn} and holes, E_t , $E_{tp} < E < E_{tn}$.

The position of quasi-Fermi level for trapped electrons, E_{tn} [35, 36], is determined from the measured dc photocurrent at applied bias voltage and under constant illumination from Eq. (8) in [36]. At E_{tn} and $E_{tp,}$ the occupation function, $f_{dc,}$ of gap states changes from 1 to 0 in two steps. The dc generation rate characteristic time response (Eq. (1) in [36]), extracted from measured photocurrent transient response is compared with the characteristic time of the experiment, taking in to account the characteristic capture frequency ω_c (Eq. (2) in [36]) to determine the high or low frequency regime of the experiment.

From calculated values, in our experiment, the chosen frequency falls in the low-frequency regime. In this regime, only the defects around the Fermi level can be probed. The requirement

that Fermi level of free electrons coincides with quasi-Fermi level of trapped electron will be satisfied.

The measured a-Si:H p-i-n photodiode switch-off photocurrent transient response on blue probe light at blue bias light and 0 V bias voltage on 10 kΩ load resistor, the calculated transient response, and difference between them are shown in **Figure 9**. The two exponential functions, as in **Figure 9**, are present in all the cases of applied bias voltage.

Figure 10 shows the numerically extracted energies of localized states from measured photocurrent transient response. The weighting factor (pre-exponential factor) of localized states is shown in **Figure 11**. The weighting factors corresponding to the deeper gap states (E_2) are higher than those of the shallower (E_1) states for all voltages below the built-in voltage. With increasing forward bias voltage, there is an increase in weighting factor corresponding to energy E_1 and decrease in those of energy E_2. The energy levels E_1 and E_2 shift toward deeper energy levels for moderate forward voltages below the built-in voltage. At high forward voltages, both shift toward shallower values. This is in agreement with [27], where the capture coefficients of the midgap states were higher than those of the shallow localized states. Also, these results confirm the capacitance upper limit described above (**Figures 7** and **8**).

2.4. a-Si:H p-i-n photodiode as a transducer in biosensors

By definition of Mehrotra, biosensors are analytical devices that convert a biological response into an electrical signal [37]. They have many applications in medical diagnostics, pharmaceutical, food, beverage, agricultural, environmental, and biotechnological industries. Two main components of biosensors are the bioreceptor and transducer [38, 39]. Bioreceptor is a

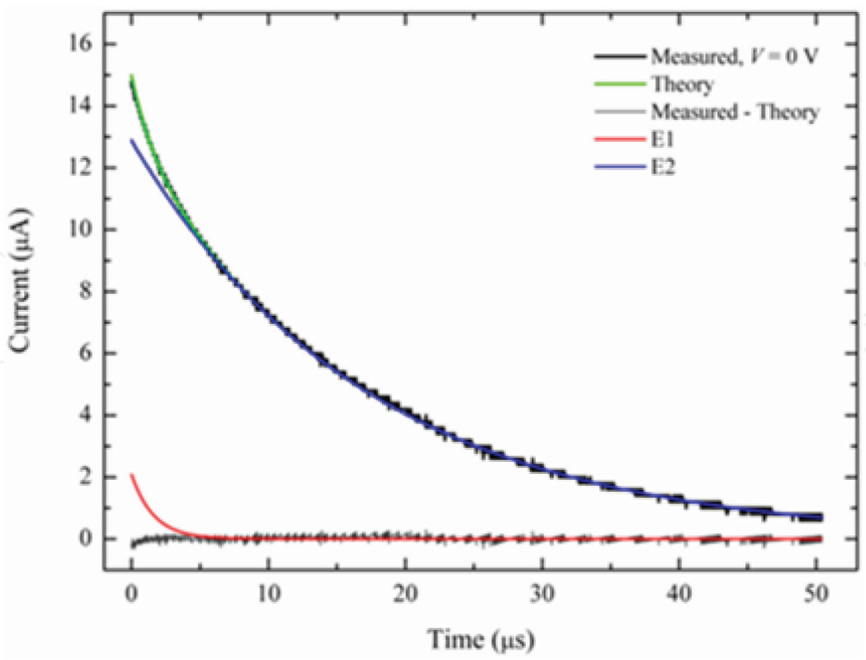

Figure 9. The measured a-Si:H p-i-n photodiode switch-off photocurrent transient response on blue probe light at blue bias light and 0 V bias voltage on 10 kΩ load resistor, the numerically reconstructed transient response (theory), and difference between them.

http://dx.doi.org/10.5772/intechopen.80503

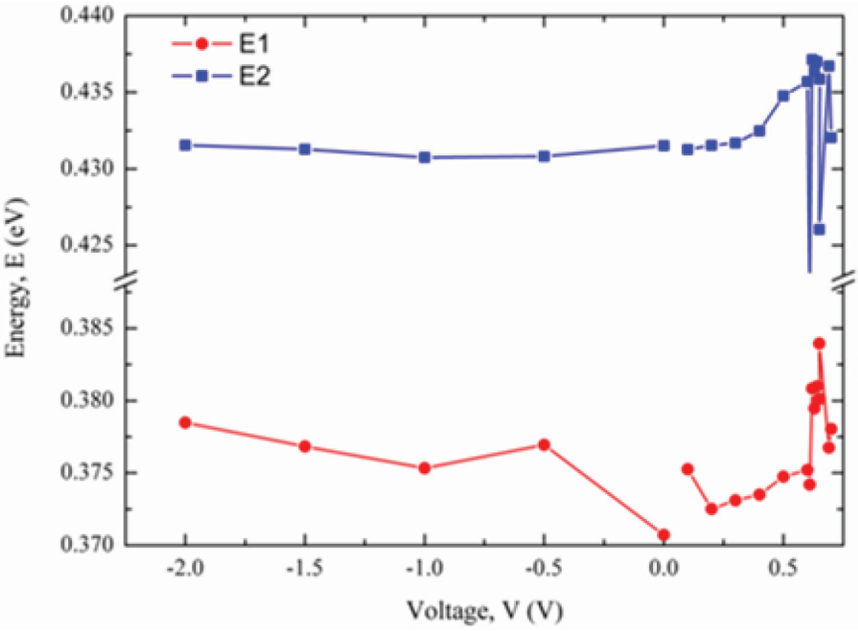

Figure 10. The energies of localized states extracted from measured photocurrent transient response of a-Si:H p-i-n PD on blue probe light at blue bias light at applied voltages Vappl. = −2 to 0.7 V.

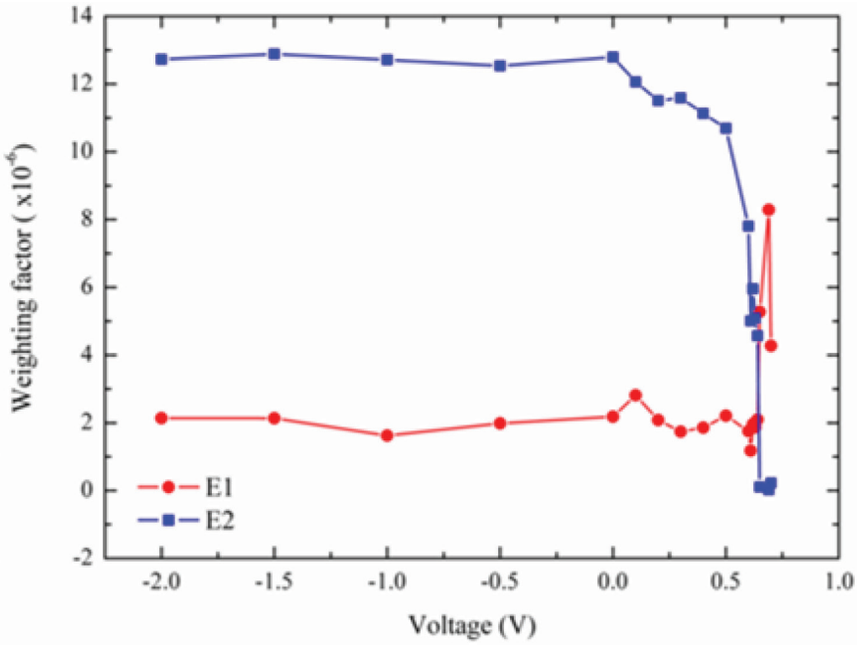

Figure 11. Weighting factor of localized states extracted from measured photocurrent transient response of a-Si:H p-i-n PD on blue probe light at blue bias light at applied voltages Vappl. = −2 to 0.7 V.

part that recognizes the analyte of interest, while biotransducer is a physicochemical detector that converts the bioreceptor-analyte complex into a measurable signal. As the name says, a bioreceptor is a biological molecule like enzymes, antibodies, and nucleic acid, but it can also be a tissue, organelle, or microorganism, while the biotransducer's measurable signal may be viscosity, mass, temperature, electrical current, electrical potential, impedance, conductance,

electromagnetic field, electromagnetic radiation, or visible light. Biosensors can be label-free or label based which depends on their detection system [40].

Biosensing elements can be described as follows:

Enzymes: protein molecule which acts as a catalyst in chemical reactions. They can be mobilized on transducers by gel entrapment technology, covalent binding, or physical adsorption.

Microbes: they are capable of transforming analytes to specific products which can be monitored by transducer.

Organelle: more specific for analysis.

Antibodies: highly selective to antigens and can be attached to matrix surface of transducer.

Nucleic acids: are DNA and RNA molecules which can be hybridized with other nucleic acids, so it can be a good sensing element for metabolic disorders, infection disease, cancer, and genetic disorders.

Aptamers: those are single-stranded DNA or RNA molecules and can be specific against amino acids, proteins, and other molecules by adopting specific and stable secondary structures against mentioned analytes.

Biosensors can be classified as electrochemical, mass dependent, optical, radiation sensitive [39], or piezoelectric based on their transduction principle. Based on the detected analyte, they can be immunosensors, aptasensors, genosensors, or enzymatic biosensors.

Optical biosensors have light as the output transducer signal. Light is generated by optical diffraction and electrochemiluminescence as main mechanisms for light production [41]. Bioluminescence is a process in which biomolecules absorb light, from the excitation source and enter into excited state, then fall down to the ground state and emit light as fluorescence or phosphorescence. Chemiluminescence is a type of luminescence when the light is emitted by chemical reaction. If the chemical reaction is catalyzed by an enzyme, it is called bioluminescence [42].

Regard, their above described characteristics, the a-Si:H photodiodes have become driving force in the scientific community for detection of tumor cells. For in vitro testing of HeLa cells, it is important to note that:

1. Cells are standardly grown in complemented Dulbecco's Modified Eagle Medium (DMEM) with fetal bovine serum addition.
2. For counting, cells are removed from the surface plate by use of enzyme trypsin.
3. All the components (cells, DMEM, and trypsin) absorb blue light.

DMEM (Dulbecco's Modified Eagle Medium) has been proposed for culturing normal and tumor cells. Constituents of the medium are high level of glucose, essential minerals, amino acid, and vitamins. Alone, it does not function for cell culturing; so, it must be complemented with fetal bovine serum, antibiotics, and L-glutamine. The components of the complemented medium DMEM that absorb blue light are riboflavin (vitamin B12), hemoglobin, and bilirubin

[43–45]. From previous works, it is known that bilirubin and riboflavin decompose under exposure of blue light [43, 46]. There are numerous factors that influence photodegradation, like radiation source, intensity, wavelength, pH, buffer, solvent polarity, and viscosity [43]. The influence of blue light on (a) complemented DMEM medium and (b) HeLa cells can be monitored by amorphous silicon (a-Si:H) photodiodes.

The photodiode's (Department of Information Engineering, Electronics and Telecommunications, Sapienza Università di Roma, Italy) p-doped/intrinsic/n-doped junction of a:Si-H layers were deposited on 50 × 50 × 1.1 mm^3 glass substrate and arranged in 5 × 6 array. The a-Si:H layers were deposited by plasma-enhanced chemical vapor deposition (PECVD) in a three-chamber high-vacuum system. The bottom electrode is a 180–nm-thick indium tin oxide (ITO) layer. The top metal electrode is a three-metal-layer stack (30-nm-thick Cr/150-nm-thick Al/30-nm-thick Cr). The area of each photodiode is 2 × 2 mm^2. Further details on the photodiode array fabrication can be found in [47].

The a-Si:H photodiode illuminated with blue LED light (RGB LED Lamp Kingbright emitting at 430 nm) is placed in a dark metallic box. The LED current was fixed at 20 mA to provide constant illumination. A reverse bias voltage equal to 2 V was applied to the photodiode. The measurements for calibration were performed at room temperature for 1 h. Before starting the assay, the 3-ml solutions containing the appropriate concentration of HeLa cells in DMEM and DMEM, respectively, are introduced with pipette in a plastic well posted on a photodiode surface. The box is then closed to minimize room light interference. The measurements are performed at 2-V reverse bias. The photodiode current and voltage are monitored for 1 h using the Keysight BenchVue software. The photodiode is connected in series with a load resistor, R_L, of 10 kΩ, voltage source (Agilent Technologies E3631A DC voltage source), and digital multimeters, DMMs (Agilent Technologies 34450A meter). Before starting the assay, the a-Si:H photodiode is illuminated with white light to neutralize the defects induced with previous blue light illumination and to reverse the process of decreasing of photoconductivity.

The significant changes in current are observed in first 20 minutes. The current characteristic transients corresponding to blue LED-induced HeLa cells' chemiluminescence detected by a-Si:H p-i-n photodiode are shown in **Figure 12**.

It can be deduced from the **Figure 12** that the photocurrent initially decreases due to creation of two types of defects under blue light illumination. The measured photocurrent (a) when 3 mL of complemented DMEM and trypsin are placed in plastic well has faster exponential decay than the photodiode in first 2 min. The decrease in photocurrent can be attributed to absorption of blue light in the DMEM solution and in the photodiode. After 20 min, the photocurrent decreases which can be attributed to the decomposition of riboflavin (not presented here). It is also known from the literature that bilirubin and riboflavin obey first-order decomposition kinetics when they are exposed to blue light; and although the kinetic coefficient for riboflavin is 10 times greater than for bilirubin, it can be speculated that riboflavin decomposes in our experiment [46, 48].

Effects of visible spectra on live organisms have been studied for different approaches. Light can induce photochemical reactions in living cells and can have benefits in treatment of some

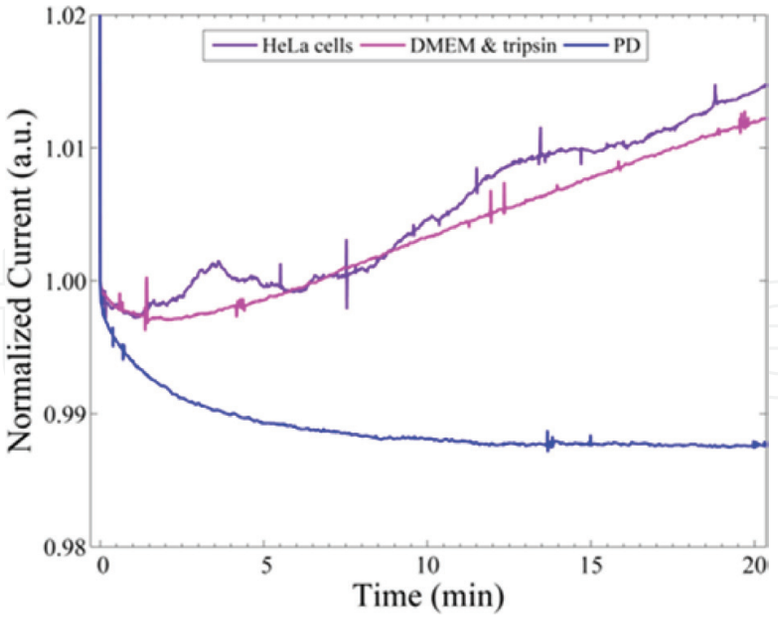

Figure 12. Normalized measured a-Si:H p-i-n photodiode, PD photocurrent versus time, with HeLa cells, and DMEM and trypsin, respectively, in plastic well on PD surface.

diseases, that is, psoriasis and neonatal hyperbilirubinemia [49, 50]. It can modulate the endocrine system and accelerate the maturation of ovaries in young rats [51].

Blue light can influence skin-keratinocytes exerting antiproliferative effect and inducing differentiation; so, it can have therapeutic effects for hyperproliferative skin conditions [52]. Effects of blue light on human health are very beneficial because it can inhibit the growth of tumors, killing bacterial spores or inactivate microorganisms [53–55]. There are a number of chromophores inside cells that absorb blue light like riboflavin, flavin proteins, iron-sulfur proteins, cytochromes, etc. a-Si:H p-i-n photodiode can be a good detector with high sensitivity, good spectral responsivity, and small reflectance for blue light, for measuring low light intensity in visible spectrum (430–780 nm). So, (b) in experiment with HeLa cells under blue light illumination the low intensity light, which is product of chemiluminescence inside cells, can be detected. According to this experiment, HeLa cells under illumination with blue light exert dramatic changes in their metabolic activity. It is well known that blue light can induce hydrogen peroxide production in mammalian cells, and release nitrogen oxide from nitrosylated proteins [52, 53]. In tumor HeLa cells, nitric oxide modulates a number of biological processes which can be witnessed by increase in NO-synthetase levels [56]. Also, it is well known that nitric oxide and hydrogen peroxide can react and release light from chemiluminescence reaction producing the toxic reactive oxygen species singlet oxygen [57]. Singlet oxygen can induce serious damage in cells and could kill 43% of tumor cells in 1 h in our experiments. So, the blue light has two effects on tumor HeLa cells: inducing chemiluminescence and killing tumor cells. Chemiluminescence can be detected by a-Si:H photodiode and that chemiluminescence reaction rate versus time sequence obeys the exponential decay. **Figure 13** shows the difference in photocurrent of HeLa cells and DMEM and trypsin. It can be deduced that absorption of HeLa cells can be separated from complemented DMEM medium. It can be

http://dx.doi.org/10.5772/intechopen.80503

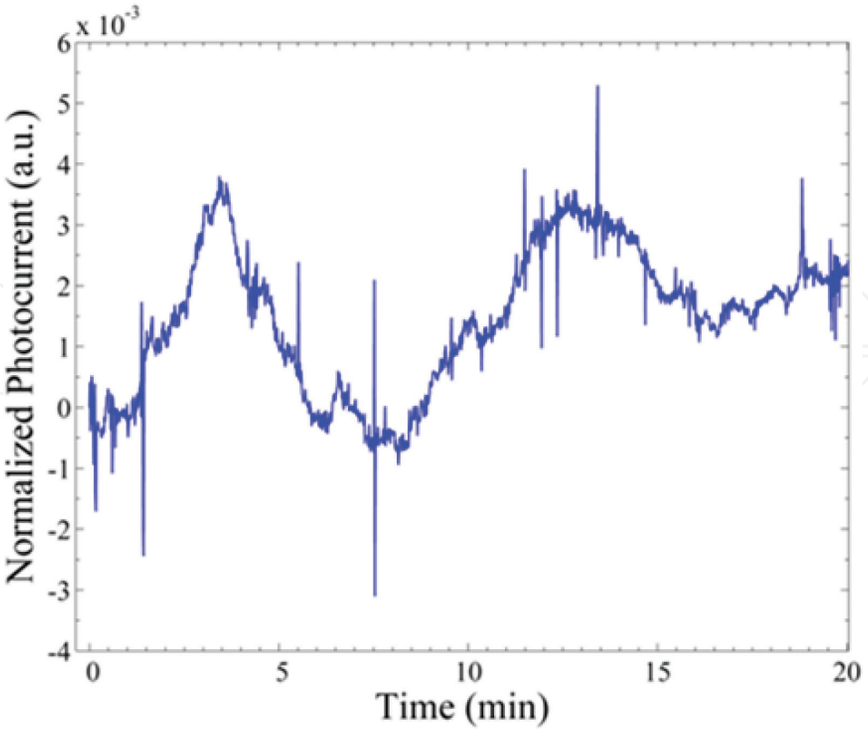

Figure 13. The normalized photocurrent difference of HeLa cells and DMEM and trypsin.

concluded that HeLa cells produce chemiluminescence radiation in the visible part of spectrum, while in the DMEM solution, this is not observed.

3. Conclusions

We performed an experiment on mammalian cells' chemiluminescence detection based on the phenomenon that under illumination of two-beam, reverse-biased a-Si:H photodiode current exceed expected primary photocurrent. The native and metastable defects in a-si:H p-i-n phtodiodes activated in this phenomenon are first characterized with simultaneous blue light pulse and constant blue light illumination at low frequency. From a transient response, the photocapacitance is analyzed. Finally, the HeLa cells' chemiluminescence reaction measurement method is done. It can be concluded that a-Si:H photodiodes can be good transducers in optical biosensors for detecting tumor cells and chemiluminescence reaction inside cells.

Acknowledgements

The authors thank Prof. Domenico Caputo and Prof. Giampiero de Cesare at University of Rome "La Sapienza", Italy and group from process line at Solar cells d.o.o. Split Croatia for provision of samples used in this work.

Conflict of interest

The authors declare that there are no conflict of interests regarding the publication of this paper.

Author details

Vera Gradišnik[1]* and Darko Gumbarević[2]

*Address all correspondence to: vera.gradisnik@uniri.hr

1 Faculty of Engineering, University of Rijeka, Rijeka, Croatia

2 Department of Biotechnology, University of Rijeka, Rijeka, Croatia

References

[1] Robbins H, Sumitomo K, Tsujimura N, Kamei T. Integrated thin film Si fluorescence sensor coupled with a GaN microLED for microfluidic point-of-care testing. Journal of Micromechanics and Microengineering. 2018;**28**:024001. DOI: 10.1088/1361-6439/aa9e6d

[2] Santos DR, Soares RRG, Chu V, Conde JP. Performance of hydrogenated amorphous silicon thin film photosensors at Ultra-Low light levels: Towards attomole sensitivities in Lab-on-Chip biosensing applications. IEEE Sensors Journal. 2017;**17**:6895-6903. DOI: 10.1109/JSEN. 2017.2751253

[3] Kamei T, Paegel BM, Scherer JR, Skelley AM, Street RA, Mathies RA. Integrated hydrogenated amorphous Si photodiode detector for microfluidic bioanalytical devices. Analytical Chemistry. 2003;**75**:5300-5305. DOI: 10.1021/ac0301550

[4] Feenstra KF, Schropp REI, Van der Weg WF. Deposition of amorphous silicon films by hot-wire chemical vapor deposition. Journal of Applied Physics. 1999;**85**:6843-6852. DOI: 10.1063/1.370202

[5] Moraes D, Anelli G, Despeisse M, Disertori G, Garrigos A, Jarron P, et al. A novel low noise hydrogenated amorphous silicon pixel detector. Journal of Non-Crystalline Solids. 2004;**338-340**:729-731. DOI: 10.1109/NSSMIC.2005.1596579

[6] Yoshida N, Shimizu Y, Honda T, Yokoi T, Nonomura S. A study of absorption coefficient spectra in a-Si:H films near the transition from amorphous to crystalline phase measured by resonant photothermal bending spectroscopy. 2008;**354**:2164-2166. DOI: 10.1016/j.jnoncrysol.2007.10.039

[7] Fossum ER. Active pixel sensors: Are CCDs dinosaurs? In: Proceedings of the SPIE 1900 Charge-Coupled Devices and Solid State Optical Sensors III; 12 July 1993. San Jose, CA, US: SPIE; 1900. pp. 2-14. DOI: 10.1117/12.148585

[8] Izadi MH, Tousignant O, Feuto Mokam M, Karim SK. An a-Si active pixel sensor (APS) array for medical X-ray imaging. IEEE Transactions on Electron Devices. 2010;**57**: 3020-3026. DOI: 10.1109/TED.2010.2069010

[9] Karim KS, Nathan A. Readout circuit in active pixel sensors in amorphous silicon technology. IEEE Electron Device Letters. 2001;**22**:469-471. DOI: 10.1109/55.954914

[10] Karim KS, Nathan A. Amorphous silicon active pixel sensor readout circuit for digital imaging. IEEE Transactions on Electron Devices. 2003;**50**:200-208. DOI: 10.1109/TED.2002.806968

[11] Shen DS, Wagner S. Transient photocurrent in hydrogenated amorphous silicon and implications for photodetector devices. Journal of Applied Physics. 1996;**79**:794-801. DOI: 10.1063/1.360827

[12] Gradišnik V, Pavlović M, Pivac B, Zulim I. Study of the color detection of a-Si:H by transient response in the visible range. IEEE Transactions on Electron Devices. 2002;**49**: 550-556. DOI: 10.1109/16.992861

[13] Gradišnik V, Pavlović M, Pivac B, Zulim I. Transient response times of a-Si:H p-i-n color detector. IEEE Transactions on Electron Devices. 2006;**53**:2485-2491. DOI: 10.1109/TED.2006.882265

[14] Fuhs W. Recombination and transport through localized states in hydrogenated amorpohus and microcrystalline silicon. Journal of Non-Crystalline Solids. 2008;**354**:2067-2078. DOI: 10.1016/j.jnoncrysol.2007.09.008

[15] Murthy VR, Dutta V. Underlying reverse current mechanisms in a-Si:H p+−i-n+ solar cell and compact SPICE modelling. Journal of Non-Crystalline Solids. 2008;**354**:3780-3784. DOI: 10.1016/j.jnoncrysol.2008.03.041

[16] Mahmood SA, Kabir MZ. Modeling of transient and steady-state dark current in amorphous silicon p-i-n photodiodes. Current Applied Physics. 2009;**9**:1393-1396. DOI: 10.1016/j.cap.2009.03.011

[17] Dhariwal SR, Rajvanshi S. Theory of amorphous silicon solar cell (a): Numerical analysis. Solar Energy Materials & Solar Cells. 2003;**79**:199-213. DOI: 10.1016/S0927-0248(02)00414-2

[18] Dhariwal SR, Rajvanshi S. Theory of amorphous silicon solar cell (b): A five layer analytical model. Solar Energy Materials & Solar Cells. 2003;**79**:215-233. DOI: 10.1016/S0927-0248(02)00415-4

[19] Dhariwal SR, Smirty M. On the sensitivity of open-circuit voltage and fill factor on dangling bond density and Fermi level position in amorphous silicon p-i-n solar cell. Solar Energy Materials & Solar Cells. 2006;**90**:1254-1272. DOI: 10.1016/j.solmat.2005.08.001

[20] Kopprio L, Longeaud C, Schmidt J. Obtainment of the density of states in the band tails of hydrogenated amorphous silicon. Journal of Applied Physics. 2017;**122**:085702. DOI: 10.1063/1.4999626

[21] Vanecek M, Kočka J, Poruba A, Fejfar A. Direct measurement of the deep defect density in thin amorphous silicon films with the "absolute" constant photocurrent method. Journal of Applied Physics. 1995;**78**:6203-6210. DOI: 10.1063/1.360566

[22] Melskens J, Smets AHM, Schouten M, Eijt SWH, Schut H, Zeman M. New insights in the nanostructure and defect states of hydrogenated amorphous silicon obtained by annealing. IEEE Journal of Photovoltaics. 2013;**3**:65-71. DOI: 10.1109/JPHOTOV.2012.2226870

[23] Melskens J, Schouten M, Santbergen R, Fischer M, Vasudevan R, vanderVlies DJ, et al. In situ manipulation of the subgap states in hydrogenated amorphous silicon monitored by advanced application of Fourier transform photocurrent spectroscopy. Solar Energy Materials & Solar Cells. 2014;**129**:70-81. DOI: 10.1016/j.solmat.2014.03.022

[24] Jiao L, Liu H, Semoushikina S, Lee Y, Wronski CR. Initial, rapid light-induced changes in hydrogenated amorphous silicon materials and solar cell structures: The effects of charged defects. Applied Physics Letters. 1996;**69**:3713. DOI: 10.1063/1.117198

[25] Melskens J, Schouten M, Mannheim A, Vullers AS, Mohammadian Y, Eijt SWH, et al. The nature and the kinetics of light-induced defect creation in hydrogenated amorphous silicon films and solar cells IEEE. Journal of Photovoltaics. 2014;**6**:1331-1336. DOI: 10.1109/JPHOTOV.2014.2349655

[26] Zollondz J-H, Reynolds S, Main C, Smirnov V, Zrinscak I. The influence of defects on response speed of high gain two-beam photogating in a-Si:H PIN structures. Journal of Non-Crystalline Solids. 2002;**299-302**:594-598. DOI: 10.1016/S0022-3093(01)01204-2

[27] Pomoni M, Kounavis P. Determination of trapping–detrapping events, recombination processes and gap-state parameters by modulated photocurrent measurements on amorphous silicon. Philosophical Magazine. 2015;**94**:2447-2471. DOI: 10.1080/14786435.2014.914262

[28] Gradišnik V, Jeričević Ž. The a-Si:H device characteristics degradation upon the light induced defects. In: Book of Abstracts of the 3rd Euroregional Workshop on Photovoltaics & Nanophotonics 2016 (EUROREG PV 2016); 21-23 September 2016; Lubljana. Slovenia: LPVO Faculty of Electrical Engineering; 2016. p. 21

[29] Han D, Melcher DC, Schiff EA. Optical-bias effects in electron-drift measurements and defect relaxation in a-Si:H. Physical Review B. 1993;**48**:8658-8666. DOI: 10.1103/PhysRevB.48.8658

[30] Kind R, van Swaaij RAACMM, Rubinelli FA, Solntsev S Zeman M. Thermal ideality factor of hydrogenated amorphous silicon p-i-n solar cells. Journal of Applied Physics. 2011;**110**:104512. DOI: 10.1063/1.3662924

[31] Deng J, Wronski CR. Carrier recombination and differential diode quality factors in the dark forward bias current-voltage characteristics of aSi:H solar cells. Journal of Applied Physics. 2005;**98**:024509. DOI: 1063/1.1990267

[32] Kumar RA, Suresh MS, Nagaraju J. Time domain technique to measure solar cell capacitance. Review of Scientific Instruments. 2003;**74**:3516-3519. DOI: 10.1063/1.1582391

[33] Čović M, Gradišnik V, Jeričević Ž. The investigation of influence of localized states on a-Si:H p-i-n photodiode transient response to blue light impulse with blue light optical bias. In: Proceedings of the 39th International Convention on Information and Communication Technology, Electronics and Microelectronics (MIPRO 2016); 30 May-3 June 2016; Opatija. Croatia: IEEE; 2016. pp. 24-27. DOI: 10.1109/MIPRO.2016.7522104

[34] Jericevic Z. Method for Fitting a Sum of Exponentials to Experimental Data by Linearization Using Numerical Integration Approximation, and Its Application to Well Log Data. [US Patent] USP #7,088,097; 2006

[35] Kounavis P. Changes in the trapping and recombination process of hydrogenated amorphous silicon in the Staebler–Wronski effect. Journal of Applied Physics. 1995;**77**: 3872-3878. DOI: 10.1063/1.358565

[36] Kleider J-P, Longeaud C, Gueunier M-E. The modulated photocurrent technique: A powerful tool to investigate band gap states in silicon based thin films. Physica Status Solidi (C). 2004;**1**:1208-1226. DOI: 10.1002/pssc.200304322

[37] Mehrotra P. Biosensors and their applications—A review. Journal of Oral Biology and Craniofacial Research. 2016;**6**:153-159. DOI: 10.1016/j.jobcr.2015.12.002

[38] Darsanaki RK, Azizzadeh A, Nourbakhsh M, Raeisi G, Aliabadi MA. Biosensors: Functions and applications. Journal of Biology and Today's World. 2013;**2**:53-61. DOI: 10.15412/J.JBTW.01020105

[39] Ali J, Najeeb J, Ali MA, Aslam MF, Raza A. Biosensors: Their fundamentals, designs, types and most recent impactful applications: A review. Journal of Biosensors and Bioelectronics. 2017;**8**:9. DOI: 10.4172/2155-6210.1000235

[40] Vigneshvar S, Sudhakumari CC, Senthilkumaran B, Prakash H. Recent advances in biosensor technology for potential applications—An overview. Frontiers in Biotechnology and Bioengenieering. 2016;**4**:11. DOI: 10.3389/fbice.2016.00011

[41] Duval D, Lechuga LM. Breakthroughs in Photonics 2012: 2012 Breakthroughs in Lab-on-a-Chip and Optical Biosensors. IEEE Photonics Journal. 2013;**5**. DOI: 10.1109/JPHOT.2013.2250943

[42] Nabi A. Instrumentation for chemiluminescence and bioluminescence assays (Part-I). Journal Chemical Society of Pakistan. 1991;**13**:90-95

[43] Sheraz MA, Kazi SH, Ahmed S, Anwar Z, Ahmad I. Photo, thermal and chemical degradation of riboflavin. Beilstein Journal of Organic Chemistry. 2014;**10**:1999-2012. DOI: 10.3762/bjoc.10.208

[44] Horecher BL. The absorption spectra of hemoglobin and its derivatives in the visible and near infra-red regions. Journal of Biological Chemistry. 1943;**148**:173-183

[45] McDonagh AF, Palma LA, Lightner DA. Blue Light and Bilirubine Excretion. Science. 1980;**208**:145-151. DOI: 10.1126/science.7361112

[46] Ahmad HB, Ahmad S, Shad MA, Hussain M. Kinetic measurement of photodecomposition of bilirubin. Asian Journal of Chemistry. 2013;**25**:7945-7948. DOI: 10.14233/ajchem.2013.14749

[47] Constantini F, Sberna C, Petrucci G, Reverberi M, Domenici F, Fanelli C, et al. Aptamer-based sandwich assay for on chip detection of Ochratoxin A by an array of amorphous silicon photosensors. Sensors and Actuators B: Chemical. 2016;**230**:31-39. DOI: 10.1016/j.snb.2016.02.036

[48] Sattar A, de Man JM, Alexander JC. Light-Induced degradation of Vitamins I. Kinetic studies of riboflavin decomposition in solution. Canadian Institute of Food Science and Technology journal. 1977;**10**:61-64. DOI: 10.1016/S0315-5463(77)73439-X

[49] Ferguson J. A controlled study of ultraviolet A sunbed treatment of psoriasis. British Journal of Dermatology. 2000;**143**:919-920. DOI: 10.1046/j.1365-2133.2000.03820.x

[50] Salih FM. Can sunlight replace phototherapy units in the treatment of neonatal jaundice? An in vitro study. Photodermatology, Photoimmunology & Photomedicine. 2001;**17**(6):272-277. DOI: 10.1111/j.1600-0781.2001.170605.x

[51] Wurtman RJ. The effects of light on the human body. American Journal of Sciences. 1975;**233**(1):69-77. DOI: 10.1038/scientificamerican0775-68

[52] Liebmann J, Born M, Kolb-Bachofen V. Blue-light irradiation regulates proliferation and differentiation in human skin cells. Journal of Investigative Dermatology. 2010;**130**(1):259-269. DOI: 10.1038/jid.2009.194

[53] Sparsa A, Faucher K, Sol V, Durox H, Boulinguez S, Doffoel-Hantz V, et al. Blue light is phototoxic for B16f10 murine melanoma and bovine endothelial cell lines by direct cytocidal effect. Anticancer Research. 2010;**30**(1):143-148

[54] Denis TGS, Dai T, Hamblin MR. Killing bacterial spores with blue light: When innate resistance meets the powerof light. Photochemistry and Photobiology. 2013;**89**(1):2-4. DOI: 10.1111/j.1751-1097.2012.01233.x

[55] Liang J-Y, Yuann J-MP, Cheng CW, Jian HL, Lin C-C, Yu Chen L. Blue light induced free radicals from riboflavin on *E. coli* DNA damage. Journal of Photochemistry and Photobiology B: Biology. 2013;**119**:60-64

[56] Choudhari SK, Chaudhary M, Badge S, Gadbail AR, Joshi V. Nitric oxide and cancer: A review. World Journal of Surgical Oncology. 2013;**11**:1-11. DOI: 10.1186/1477-7819-11-118

[57] Noronha-Dutra AA, Epperlein MM, Woolf N. Reaction of nitric oxide with hydrogen peroxide to produce potentially cytotoxic singlet oxygen as a model for nitric oxide-mediated killing. FEBS Letters. 1993;**321**:59-62. DOI: 10.1016/0014-5793(93)80621-Z